



OPEN

SUBJECT AREAS:

MECHANICAL  
ENGINEERING

POLYMERS

COMPOSITES

MECHANICAL PROPERTIES

Received

31 December 2012

Accepted

3 June 2013

Published

24 June 2013

Correspondence and  
requests for materials  
should be addressed to  
P.K. (praveenk@  
materials.iisc.ernet.in)

# Periodic Architecture for High Performance Shock Absorbing Composites

Abha Misra<sup>1</sup> & Praveen Kumar<sup>2</sup>

<sup>1</sup>Department of Instrumentation and Applied Physics, <sup>2</sup>Department of Materials Engineering, Indian Institute of Science, Bangalore 560012 (India).

A novel composite architecture consisting of a periodic arrangement of closely-spaced spheres of a stiff material embedded in a soft matrix is proposed for extremely high damping and shock absorption capacity. Efficacy of this architecture is demonstrated by compression loading a composite, where multiple steel balls were stacked upon each other in a polydimethylsiloxane (PDMS) matrix, at a low strain-rate of  $0.05 \text{ s}^{-1}$  and a very high strain-rate of  $>2400 \text{ s}^{-1}$ . The balls slide over each other upon loading, and revert to their original position when the load is removed. Because of imposition of additional strains into the matrix via this reversible, constrained movement of the balls, the composite absorbs significantly larger energy and endures much lesser permanent damage than the monolithic PDMS during both quasi-static and impact loadings. During the impact loading, energy absorbed per unit weight for the composite was  $\sim 8$  times larger than the monolithic PDMS.

Composites are often prepared with multiple constituents having widely different properties to meet critical requirements of an application. The desired properties of composites are sometimes contradictory, and attainment of these properties often involves design of novel material architectures, such as placement of a few volume fraction of percolating carbon nanotubes (CNTs), nano-sized metallic wires, etc. in a non-conducting soft matrix, like polymers, etc. to achieve different functionalities such as flexible electrical conductors<sup>1–3</sup>, uniform placement of particulates of a high conducting-high melting material, such as Cu, in continuous channels of mechanically soft matrix, such as In, for enhancing the thermal conductivity of a composite while maintaining the high compliance<sup>4,5</sup>, etc. The common theme in these efficient architectures is the controlled placement of different constituents adhering to a specified design; this allows efficient division of the functionality amongst the constituents leading to the desired behavior of the material. This work proposes a novel architecture for manufacturing composites with superior damping and shock absorption properties.

Elastomeric polymers based composites are important damping and shock absorption materials<sup>6–9</sup>. A few tunable properties of polymers, such as the ability to endure very large strains<sup>9,10</sup>, high energy absorption to weight ratio<sup>7</sup>, easy placement of a continuous coating on large structures<sup>9</sup>, etc., have made polymer based composites as the material of choice for shock absorption applications<sup>7</sup>. Various composites, such as carbon-black, SiC and other nanoparticles reinforced polymers<sup>1,10–14</sup>, laminated composites with interlayers of polymers and metals<sup>6,15,16</sup>, and polymers reinforced with fibers of glass, carbon and specialized polymers<sup>17,18</sup>, etc., have been particularly developed to improve the damping properties of monolithic polymers. This improvement primarily occurs through increase of one or a combination of more of the following: (i) number of the micro-fracture sites, (ii) volume fraction of the strain induced crystallites in the polymer matrix, and (iii) the strength of the composites without compromising its strain endurance limit. However, one of the inherent drawbacks in these composites is that their improved properties are based on a certain combination of particular materials and therefore they do not have the generality of the architecture or the specific design based composites. The latter allows tailoring the properties of a composite by placing the micro-constituents in a certain fashion; this provides an additional valuable tool for further improving the damping and shock absorbing capabilities of even an existing composite material. This work proposes and validates the damping and shock absorbing capability of a composite architecture consisting of a chain like periodic inclusions of a stiff material into a polymer matrix.

## Results

**Quasistatic behavior.** Figure 1a, b show stress-strain behavior of monolithic polydimethylsiloxane (PDMS) during the first and the second loading-unloading cycles, respectively. A finite non-zero stress-strain

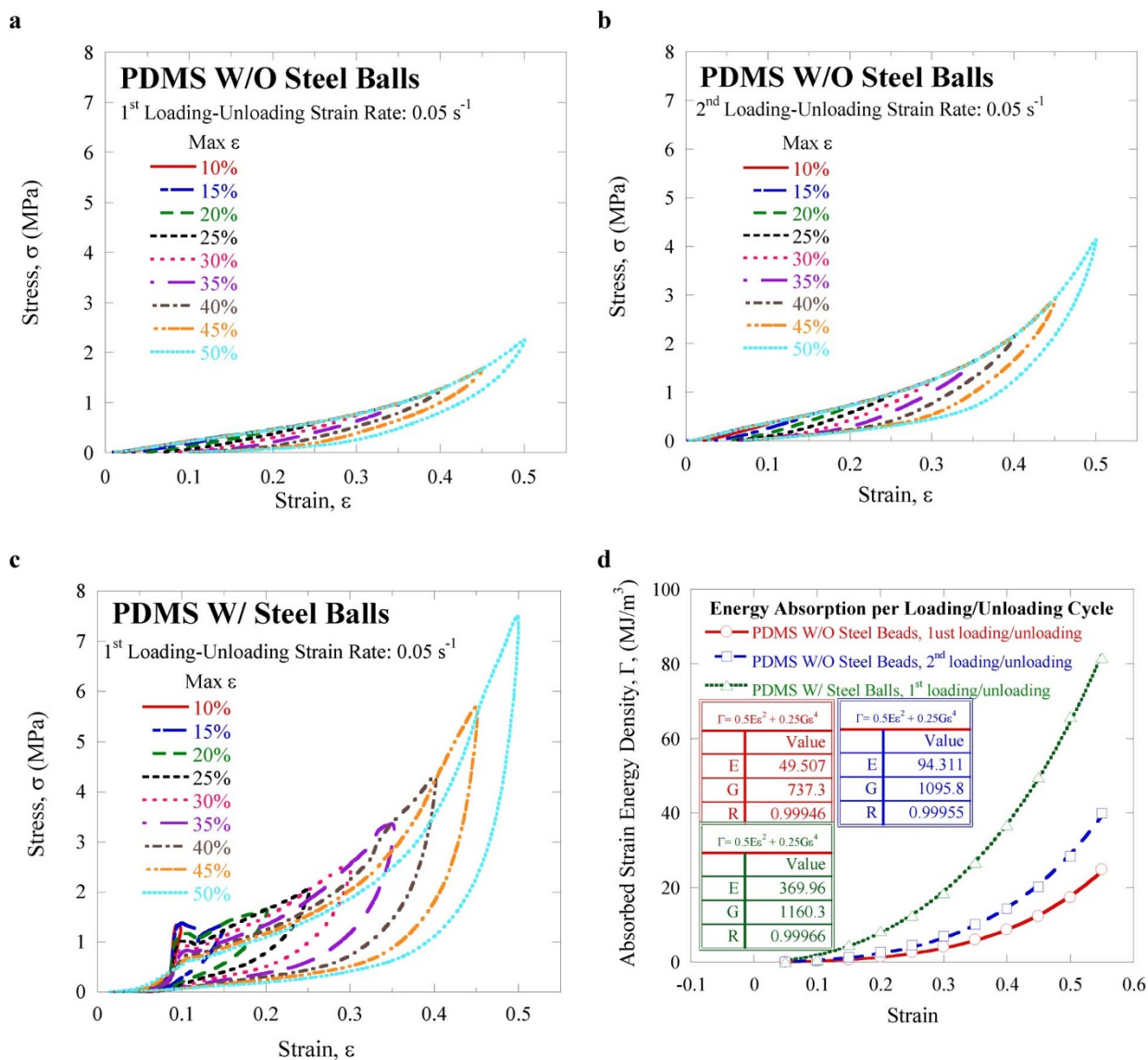


**Figure 1** | Stress-strain behavior of PDMS with and without steel balls embedded in it. (a) Monolithic PDMS samples during the first loading-unloading cycle. (b) monolithic PDMS samples during the second loading-unloading cycle. (c) PDMS – steel ball composite during the first loading-unloading cycle. (d) energy dissipated due to the stress-strain hysteresis for all samples tested at the strain rate of 0.05 per s. A best fit curve analysis of (d) with equation,  $\Gamma = 0.5E\epsilon^2 + 0.25G\epsilon^4$  results  $E$  and  $G$  parameters in the units of MJ/m<sup>3</sup> as 49.507 and 737.3, 94.31 and 1095, and 369.96 and 1160 for PDMS samples during the first loading-unloading, PDMS sample during the second loading-unloading and PDMS-steel ball composite during the first loading-unloading, respectively. As compared to the maximum stress during the first loading-unloading cycle of PDMS sample, the stresses at a strain for the 2<sup>nd</sup> loading-unloading of PDMS and 1<sup>st</sup> loading-unloading of PDMS-steel ball composites were  $\sim 1.7 \pm 0.1$  and  $3.5 \pm 0.2$ , respectively, times larger. Different samples were tested for each test (*i.e.* maximum strain condition).

hysteresis was observed in the samples even compressed only up to a strain of 5%; this indicates that the polymer chains in these PDMS samples started to non-conservatively compress<sup>10</sup>, glide over each other<sup>10</sup> and form stable strain-induced crystallites, as reported in several thermo-plastics<sup>19,20</sup> including PDMS based composites<sup>20</sup>, right at the onset of the deformation. Furthermore, a close inspection of the stress-strain plot reveals ideal rubbery behavior of the PDMS samples consisting of the two distinct regimes: (i) the stress-strain plots were linear up to the strains of  $\sim 20$  to 25%, and (ii) the stress-strain behavior became non-linear at higher strains, where the stress increased rapidly with the strain. Nominal values of Young's modulus were calculated from the slope of the linear region of curves and were equal to 2.2 and 3.6 MPa, respectively for the first and the second loadings. Also, irrespective of the maximum strain incurred during the first loading, the maximum stress as well as the

stress-strain hysteresis during the second loading-unloading cycle became bigger as compared to the first loading-unloading cycle. These additional observations also confirm the onset of the irreversible polymer chain stretching, gliding and formation of stable strain-induced crystallites during the loading – accumulation of these makes the sample stronger during the subsequent loading.

Figure 1c shows stress-strain behavior of the PDMS-steel ball composites during a loading–unloading cycle; different samples were compressed up to different maximum strains (10–50%). Comparison of Fig. 1a, c clearly indicates that the maximum stress sustained by these composites during any strain cycle was much higher than the monolithic PDMS. Similar to the monolithic PDMS samples, the stress behavior of the composite material consisted of a linear region followed by a non-linear region; however, the linear region for the composite materials was much smaller (less than 10%) than that of



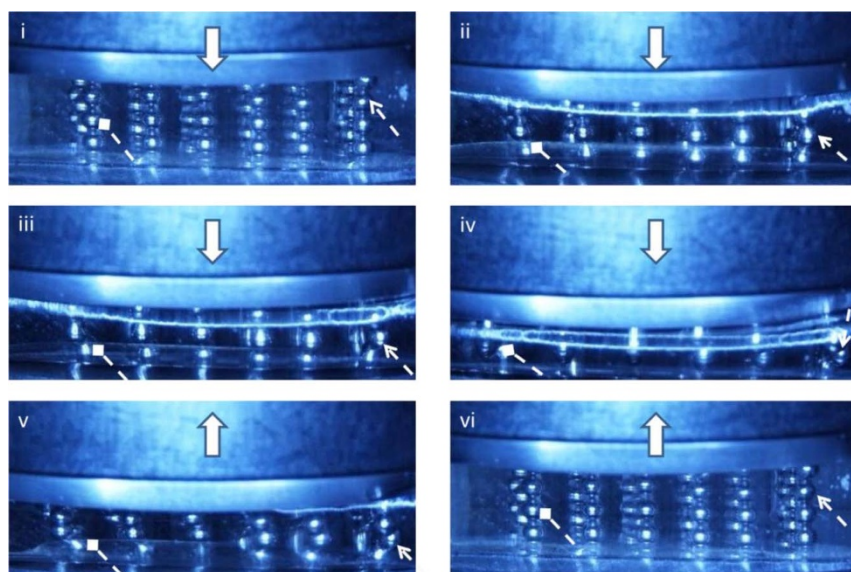
the monolithic PDMS samples. Young's modulus, as calculated from the linear region of the stress-strain plot of the PDMS-steel ball composites, was in between 3.8 and 6.8 MPa, which was almost 2 to 3 times more than that of the monolithic PDMS sample. It is interesting to note that Young's modulus of these composites, which contained almost 60% of steel, was only 2 to 3 times larger than that of PDMS. This will be explained later while discussing the deformation mechanism of these composites.

Figure 1d compares the total strain energy dissipated during a stress-strain hysteresis of the monolithic PDMS and the PDMS-steel ball composites. For all the samples tested in this study, the energy dissipated during the hysteresis seems to non-linearly depend on the maximum imposed strain. Consistent with the aforementioned observation of the larger stress-strain hysteresis for the PDMS-steel ball composites, Figure 1d also shows much larger energy dissipation in the PDMS-steel ball composites at any strain. Moreover, the non-linearity in the composite material is much larger as compared to the PDMS samples. This shows that the performance of the composites for the damping or shock absorption becomes more efficient at larger strains; this being a major advantage associated with this novel architecture over the base material and the detailed physical mechanism for the same will be discussed later.

Figure 2 shows the time-sequence photographs of a composite during loading and unloading segments of a test (refer to supplemental material 1 for videos showing the movement of steel balls during deformation). Following the sequential photographs of two balls, highlighted with broken arrows, whose motion can be considered to be on the plane normal to the camera line-of-sight, reveals that the steel balls did not deform during the loading-unloading cycle, and only slid over each other. Perhaps, the occurrence of a small peak in the stress-strain profile of these ball filled PDMS composites at the strain near the onset of non-linearity (i.e.,  $\sim 6\text{--}8\%$  of strain), as shown in Fig. 1c, corresponds to the initiation of the sliding phenomenon. Since the steel balls did not deform and only slid over each other, the composite became only  $\sim 3$  times stronger than the PDMS even though the volume fraction of the steel was  $\sim 60\%$ . The additional strength in the PDMS-steel ball composite can be attributed to the deformation of additional volume of the PDMS due to the movement of the steel balls away from their original position. The visible recovery of the original stacking following the complete

removal of the load (Fig. 2i, vi) indicates that the movement of the steel balls was completely reversible, macroscopically. Based on the facts that the stacking of the steel ball was fully recovered and the energy absorption capacity of the monolithic PDMS was enhanced during the sequential loadings (as shown in Fig. 1), it can be speculated that the energy absorption capability of the PDMS-steel ball composites would improve in the sequential loadings.

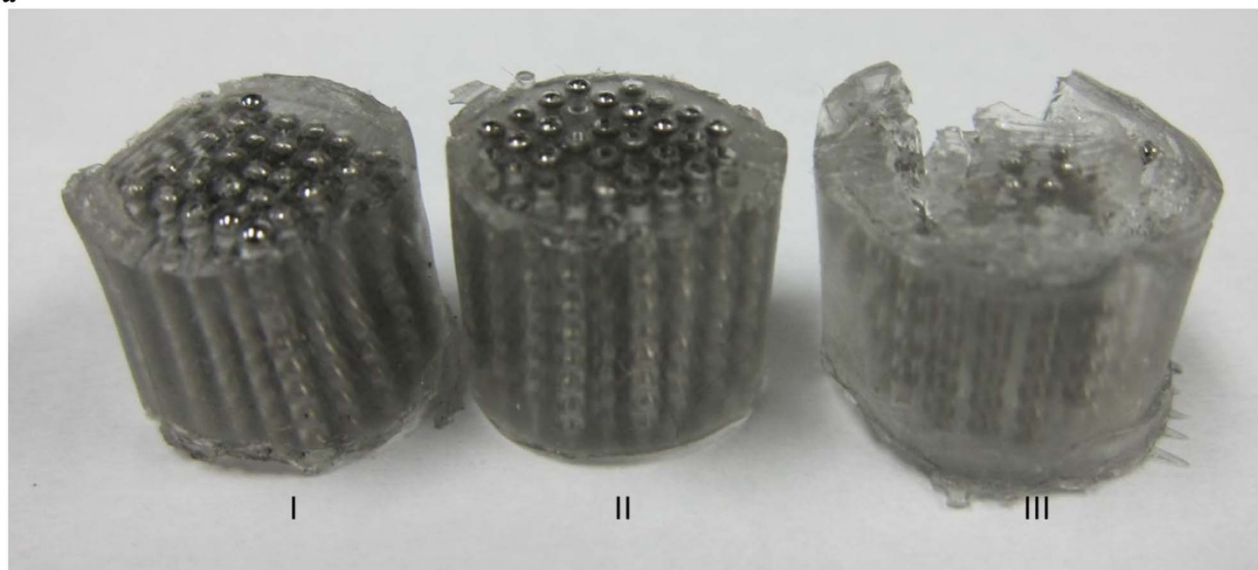
**High strain rate behavior.** Figure 3 shows the mechanical response of the PDMS and the composite under dynamic loading, imposed during a split Hopkinson bar test. Fig. 3a shows a few examples of the PDMS-steel ball composite samples following one instance of the dynamic loading. Except for a few samples, as shown in Fig. 3a-III, most of the composite samples showed insignificant accumulation of macroscopic damages during dynamic loading. On the other hand, the structural integrity of all monolithic PDMS samples was compromised, and the cylindrical samples of  $\sim 1$  aspect ratio turned into thin broken discs following one instance of dynamic loading. A few representative strain rate versus time plots are shown in Fig. 3b. Consistent with the tests at the low strain rates which showed that the composites were significantly stronger than the PDMS samples, the imposed strain rates on the composites were significantly smaller than that incurred by the monolithic PDMS samples during a split Hopkinson bar test. The representative stress-strain behavior of these samples is shown in Fig. 3c. Fig. 3c clearly shows that the PDMS-steel ball composite samples not only endured much higher stresses but also accumulated significantly larger strains under the shock loading condition. Calculation of the area under the stress-strain curves reveals that the total energy absorbed by the PDMS-steel ball composite was almost 40 times larger than that of the monolithic PDMS sample. Noting that steel is only  $\sim 8$  times denser than PDMS and hence the effective density of the composite with 60% volume fraction of the steel balls was only  $\sim 5$  time larger than PDMS, a gain in energy absorption per unit weight by a factor of  $\sim 8$  is quite valuable for impact or ballistic shock absorption applications. Interestingly, Fig. 3c also shows that the peak stress in the steel ball packed PDMS composite was only  $\sim 3$  times larger than that of the monolithic PDMS, but the PDMS-steel ball composite showed  $\sim 40$  times more shock absorption capability; this property of the proposed architecture is particularly suitable for



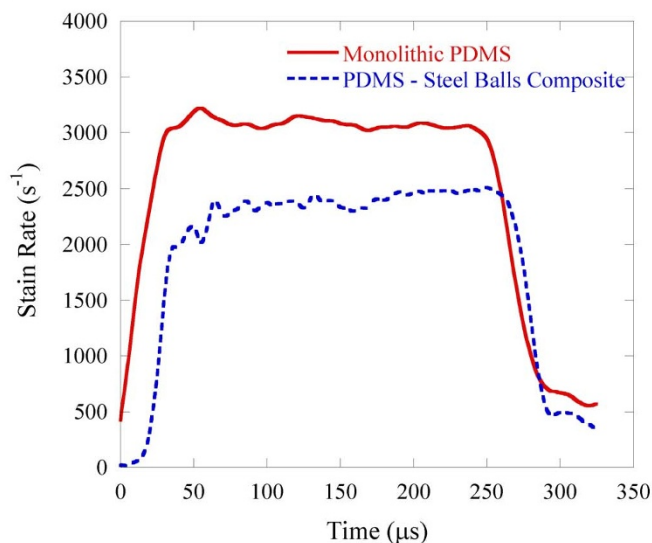
**Figure 2 | Time-sequence photographs of a shortened composite sample.** The wide arrows show the direction of loading at a given time-sequence, whereas the broken arrows show the movement of a ball as the loading and unloading occurs. One type of arrow show sequential movement of one ball. The time between different frames is not the same. Only two pictographs during unloading is shown as the unloading sequences were identical to the corresponding loading sequence.



a



b



c

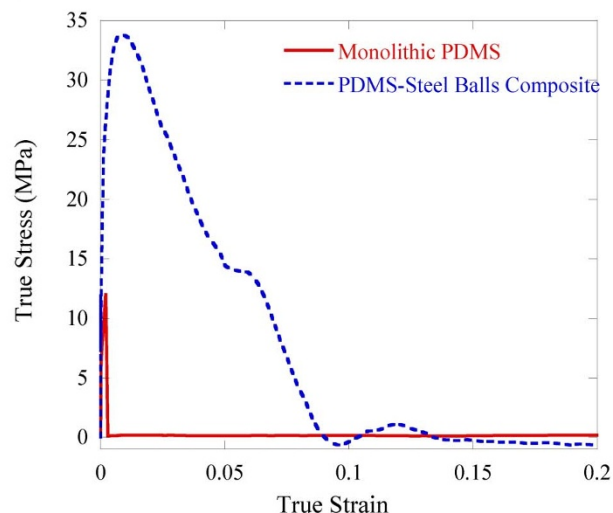


**Figure 3 | High strain rate effects on PDMS-steel ball composites.** (a) A few PDMS-steel ball composite samples following single instance of the split Hopkinson bar loading. The volume fraction of steel in I, II and III were 60%, 72% and 40%, respectively. (b) Resultant profile of the strain rate imposed on the samples during a split Hopkinson bar test. (c) Stress-strain behavior of the samples at the strain rates shown in (b).

the applications where high shock absorption is demanded with small load transfer to the attached structure, such as armor, automobile exterior, sports accessories, etc.

## Discussion

The non-linear stress-strain behavior, as observed in Fig. 1a–c, can be explained by using the standard mathematical models for the ideal rubbery materials, such as given in references 22 and 23. For strains smaller than 0.5, as relevant in this study, these models<sup>22,23</sup> can be transformed into a polynomial function. For mathematical simplicity, the following empirical polynomial stress-strain relationship was employed for the loading segment (and the unloading segment if taken separately) of the stress-strain plots:

$$\sigma = \varepsilon(a + b\varepsilon^3) \quad (1)$$

where  $\sigma$  and  $\varepsilon$  are the equivalent uniaxial stress and strain, respectively, and  $a$  and  $b$  are microstructure dependent constants, whose

physical significance is highlighted below. Table 1 shows the values of  $a$ ,  $b$  and the fitting parameter,  $R$  for all tested materials. A value of  $R$  close to 1 indicates that equation (1) aptly satisfies the stress-strain behavior of all of the tested samples. Table 1 also compares  $a$  with the value of Young's modulus,  $YM$  calculated from the linear regions of the stress-strain curves. The close similitude in the values of  $a$  and  $Young's\ modulus$  indicates that the representation, as given by equation (1), essentially treats the stress-strain behavior of these materials as the superposition of continuously occurring a linear and a non-linear (or, nonlinear elastic and marginal inelasticity) phenomenon. The linear behavior, governed primarily by the value of  $a$ , dominates the small strain response whereas the non-linear behavior, governed primarily by the value of  $b$ , is prominent at the larger strains. The observed increase in the value of  $a$ , and equivalently Young's modulus, following one cycle of loading and unloading (Table 1) is consistent with the fact that polymeric chains require more stress to be stretched following the initial partially irrecoverable stretching of the bonds and the cross-links. Since the non-linearity in the rubbery


**Table 1** | Calculated values of the parameters,  $a$  and  $b$  of equation (1) and comparison of  $a$  with the Young's modulus

Material	$a$ (MPa)	$b$ (MPa)	$R$	EM (MPa)
PDMS – 1 <sup>st</sup> Loading-Unloading	2.03	18.99	0.999	2.2
PDMS – 2 <sup>nd</sup> Loading-Unloading	3.05	39.57	0.999	3.6
PDMS-steel ball composite – 1 <sup>st</sup> Loading-Unloading	6.62	80.79	0.982	6.8
	3.85	89.00	0.997	3.8

polymers arise due to stretching of the bonds and the cross-links, sliding of the polymeric chains over each other and reduction in the open-space (or, free-volume) between the polymeric chains<sup>22</sup>, the significant increase in the value of “ $b$ ” following the first loading and unloading cycle of the monolithic PDMS can be attributed to the associated non-recoverability of the aforementioned microscopic features. It is interesting to note that the monolithic PDMS (and the PDMS-steel ball composites) did not change macroscopically following the initial loading and unloading cycles; however, the aforementioned microscopic features of these samples evolved; parameters  $a$  and  $b$  efficiently captured these microscopic changes. Therefore, the two constants of equation (1),  $a$  and  $b$ , can be thought as microstructural parameters controlling the linear and non-linear behaviors of the materials, respectively; larger the values of these parameters, stronger will be the polymer based material.

The effective resistance against deformation of the chains of the steel balls under quasistatic loading cannot be calculated using the elastic coefficients of steel because the steel balls did not deform like a monolithic material and only slid over each other during deformation; however, it can be calculated by subtracting the contribution of the PDMS from the overall response of the PDMS-steel ball composites. This can be conducted by employing isostrain analysis as the chains of steel balls are aligned in the direction of the overall deformation of the sample. The stress endured by the chains of steel ball can be given as:

$$\sigma_{steel} = \frac{\sigma_{total} - \sigma_{PDMS}f_{PDMS}}{f_{Steel}} \quad (2a)$$

$$g(\sigma)_{steel} = \frac{\sigma_{total} - g(\sigma)_{PDMS}f_{PDMS}}{f_{Steel}} \quad (2b)$$

where  $f$  is the volume fraction of a constituent,  $g(\sigma)$  is a stress function

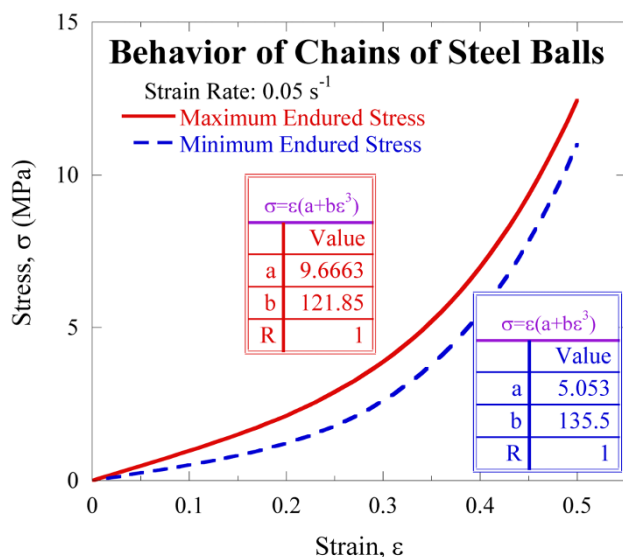


**Figure 4** | The calculation of the stresses endured by the chain of the steel balls using the isostrain condition. The maximum and the minimum endured stresses correspond to the composites which showed the maximum and the minimum loading capabilities.

and is defined as equation (1), and the subscript “steel” and “PDMS” denote the corresponding values for the chains of the steel balls and the PDMS matrix, respectively. Following the analysis based on equation (2), the load endured by the chains of the steel balls was calculated; it is shown in Fig. 4. Interestingly, the chains of the steel balls also showed an ideal rubbery behavior, as shown by the monolithic PDMS (Fig. 2a,b), with a value of  $a$  and  $b$  in the range of 5.05 to 9.66 MPa and 121.6 to 135.5 MPa, respectively.

The rubbery behavior of the chains of the steel balls, as shown in Fig. 4, can be justified through a simple analysis, which accounts for the additional stress required to displace the steel balls “sideways” into the PDMS. Figure 5a schematically shows sliding of a ball relative to another by an angle  $\theta$  from its position (shown by broken line) to a new position (shown by the continuous line). Assuming perfect sliding over the ball with center at the origin, the locus of the center of the sliding ball will follow the dotted circle, whose center coincides with the center of the stationary ball. The arrow joining the centers of the sliding and non-sliding balls will be direction of the normal force. A force balance, as shown in Fig. 5b, can relate the required force for the incurring deformation,  $F_{app}$  and the resistance due to the deformation of PDMS ( $F_{PDMS}$  and  $F_{DV}$  are the forces arising due to the uniaxial deformation of PDMS and the additional deformation of PDMS due to the sliding of the steel balls, respectively). Now, a restoring force is generated on the ball as the ball slides from its original position; the PDMS in the region, where the ball is displaced, endures a compressive stress and it tries to push the ball back to its original position, and the PDMS in the region from where the ball has moved away undergoes a tensile stress and it also tries to bring back the ball to its original position. This restoring force can be estimated by assuming that the additional strain in the PDMS due to the sideways movement of the ball scales directly to the total area of the affected PDMS,  $\Delta A$ . Thus, this additional strain in the PDMS,  $\varepsilon_{DV}$  can be given as:

$$\varepsilon_{DV} = c \frac{\Delta A}{A} = c \frac{4r^2\theta}{\pi r^2} = \frac{4c}{\pi} \theta \quad (3)$$

where  $A$  is the cross-sectional area of the sliding ball,  $r$  is the radius of the ball, and  $c$  is a dimensionless scaling factor, which can be taken as the volume fraction of the steel balls for the simplicity. Since the uniaxial strain,  $\varepsilon$  is related to the sliding of the ball and is equal to  $\delta/2d$ , where  $\delta = d(1 - \cos\theta)$  is the net downward movement of the ball and  $d$  is the diameter of the ball,  $\theta$  can be given as follows:

$$\theta = \cos^{-1}(1 - 2\varepsilon) \quad (4)$$

Now substituting  $\theta$  from equation (4) into equation (3), the following gives the relationship between strain due to the displaced volume of PDMS,  $\varepsilon_{DV}$  and the uniaxial strain in the composite,  $\varepsilon$ :

$$\varepsilon_{DV} = \frac{4c}{\pi} \cos^{-1}(1 - 2\varepsilon) \quad (5)$$

Now, writing the equilibrium equation for forces in the vertical direction (Fig. 5b) and noting that  $N = F_{DV} \cot \theta$  (i.e. the force balance in the horizontal direction), the following can be derived:

$$F_{app} = \frac{F_{DV}}{\sin \theta} + F_{PDMS} \quad (6)$$

Dividing the forces by the cross-sectional area of the composite and substituting for  $\sigma$  and  $\varepsilon$  from equations (1) and (5), respectively give

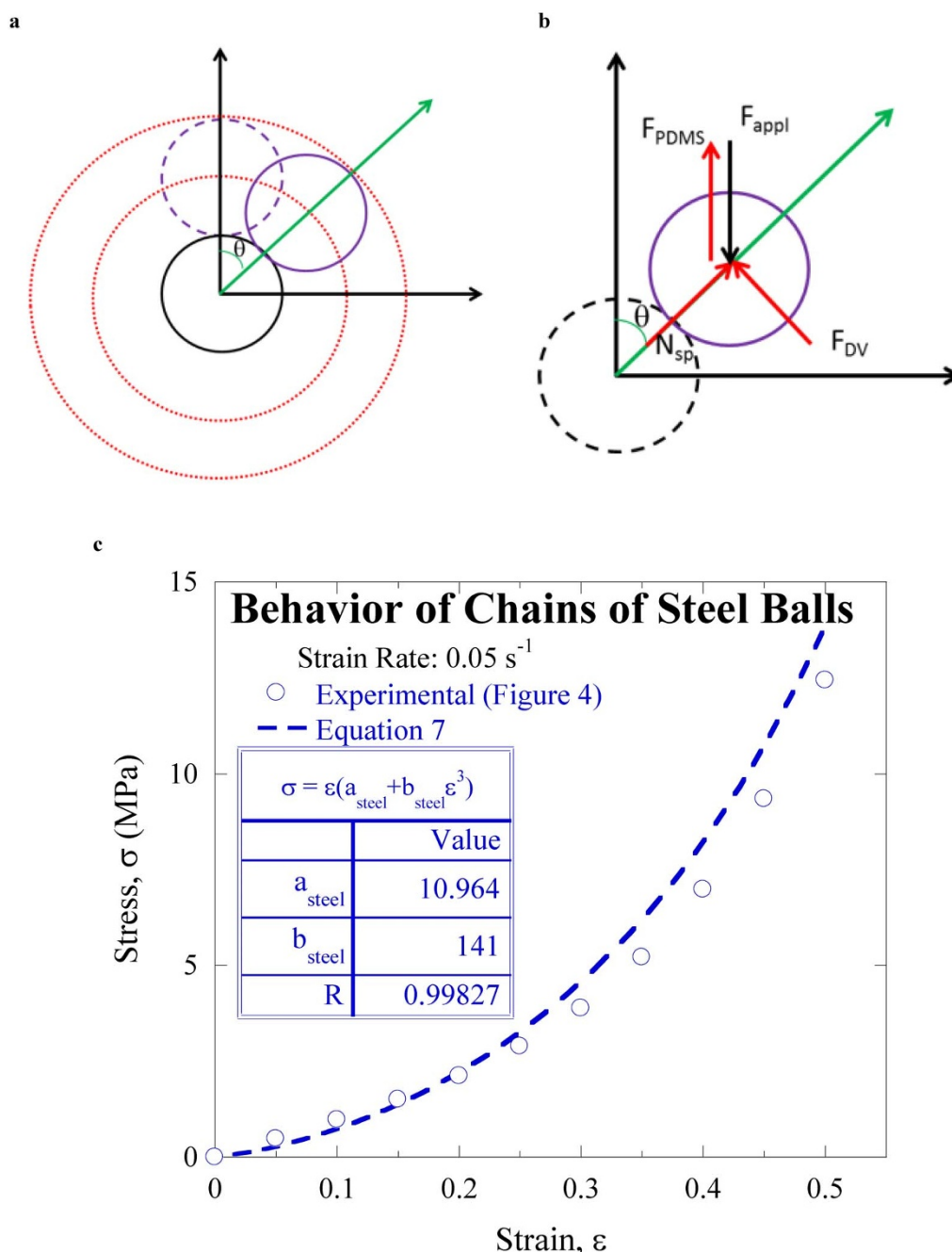


**Figure 5 | A model for ball sliding.** (a) A schematic showing the sliding motion of a steel ball over another. (b) the forces acting on the sliding ball. (c) a comparison between equation (7) and the experimental data.

the following:

$$\sigma_{app} = f_{PDMS} \left[ \varepsilon(a + b\varepsilon^3) + \frac{4c}{\pi} \frac{\cos^{-1}(1-2\varepsilon)}{\sin(\cos^{-1}(1-2\varepsilon))} \left( a + 64b \left( \frac{c}{\pi} \cos^{-1}(1-2\varepsilon) \right)^3 \right) \right] \quad (7)$$

Here the values of  $a$  and  $b$  corresponds to those of PDMS (Table 1).

Figure 5c shows the stress-strain behavior of the chains of the steel balls, as predicted by equation (7) and it also compares this prediction with the corresponding experimental data. The experimental data was back-calculated from the experiments using iso-strain analysis (i.e., Fig. 4) and indeed, there is a very good match between the experiments and equation (7). The predicted values of  $a$  and  $b$  using equations (7) are 10.96 and 141 MPa, respectively, which are again

very close to the higher experimental values reported, as shown in Fig. 4. It should be noted that a close match between the model (equation (7)) and the experimentally calculated higher stiffness data is not incidental. Since the damages related to the sample preparation mostly tend to reduce the stiffness of a composite, it is usually expected that only the experimental data showing near-ideal behavior (i.e. higher stiffness in this case) would match better with the model.

The energy dissipation in a thermo-plastic, such as PDMS, and a thermo-plastic based composite may have one or a combination of more of the following origins: (i) strain-induced nucleation and growth of crystallites, which may not completely disappear while unloading, (ii) energy dissipative glide of polymeric chains over each other, (iii) fracture of polymeric bonds and micro-fracture of interfacial bonds between the inclusion and the polymer, and (iv) friction



between the sliding inclusions, as well as between inclusions and the matrix. The observation of monotonous enhancement of the strength in the non-linear region of the stress-strain plot of the monolithic PDMS as well as the PDMS-steel ball composite (Fig. 1a–c) suggest occurrence of the strain-induced crystallization of the PDMS matrix, as reported in other thermo-plastic based materials including PDMS based composites<sup>19,20</sup>. The formed crystallites remained stable during unloading, as revealed by the steeper slope during the initial unloading (Figure 1a–c)<sup>21</sup>. This hypothesis is further supported by the higher stress as well as larger hysteresis during the second loading-unloading cycle of the monolithic PDMS samples as compared to the first loading-unloading cycle. For the PDMS-steel composite, equation (5) predicts that the strain in the PDMS, especially in the regions close to steel balls, will sustain much higher strains as the steel balls slide over each other. This is also supported by the early onset of the non-linearity in these samples (Fig. 1c). Therefore, the strain-induced crystallization of PDMS will be more vigorous in the PDMS-steel ball composite; this dramatically enhances the energy dissipation in these composites as compared to the monolithic PDMS. Nevertheless, the stresses in the PDMS region in the vicinity of the sliding balls are also very high (equations 1, 5), and this will also increase the severity of the energy dissipative glide of the polymeric chains, as well as fracture of polymeric bonds in these regions; this deformation behavior is consistent with the observation of localization of deformation in the narrow ligaments in thermoplastic vulcanizate<sup>24</sup>. Furthermore, the friction between the sliding steel balls as well as between the steel balls and the adjacent polymer will add on to the net dissipation of the strain energy in the PDMS-steel ball composite. Since the surface of the steel balls were very smooth (chrome plated) as well as contact area between steel balls was very small, the majority of the friction-induced dissipative energy would be produced due to the sliding between the steel balls and the PDMS. Friction between PDMS and steel balls depends on the shearing and fracture of the adhesion bonds between the contacting surfaces, and the plastic deformation as well as abrasion of the asperities<sup>25</sup>. Since the steel balls were mechanically implanted inside the PDMS matrix, the contribution from shearing and fracture of adhesion bonds between the contacting surfaces to the total dissipation energy should be negligible as compared to the deformation and the abrasion of PDMS asperities. Furthermore, since the friction force between steel balls and the PDMS increases with the normal (and equivalently, the applied) force<sup>25</sup> and the loading rate<sup>26</sup>, the energy dissipation due to this mechanism will greatly enhance at higher loads and during high strain rate loadings; both aspects of this dissipative mechanism is highly desirable in a shock absorption and damping application. Although the quantification of the relative contributions of the aforementioned different energy dissipative mechanisms is beyond the scope of the present work, it is reasonable to speculate that the localized strain-induced recrystallization of the PDMS matrix and the friction between the steel balls and the PDMS may primarily be responsible for the damping and shock absorption in the materials tested in this study.

Table 2 compares the efficacy of the proposed design over some of the polymer based composites in terms of the increase in the energy absorbing capacity under quasi-static loading conditions. Clearly, the proposed design seems to be significantly superior to the other composites in terms of energy absorption per unit volume.

During high strain rate loading, a PDMS-steel ball composite could absorb much higher energy under high strain rates without any obvious degradation in its structural integrity as the high volume fraction of the steel balls, which has much higher specific heat as compared to the PDMS, absorbed significant amount of this energy; therefore, the matrix PDMS could not be heated above a temperature, where it could be irreversibly deformed. This is particularly important at high strain rates where heat generation in the polymeric structure is very high due to the high friction between the sliding polymeric chains as well as in between a steel ball and the surrounding polymeric region<sup>26</sup>. Due to the limited time available for the heat conduction (or transfer) to ambient at high strain rates, local heating is exacerbated in monolithic PDMS leading to complete melting or destruction of these samples; on the other hand, steel balls in PDMS-steel ball composite act as effective heat sink and relieve excessive heating of the composite sample. This can be further justified by critical observation of Fig. 5a, where the volume fractions of steel in three composites I, II and III were 60, 72 and 40%, respectively. The sample which showed the minimum and the maximum damage accumulation were the composites containing the maximum and the minimum volume fractions of steel. In conclusion, the extraordinary enhancement in the energy absorption capability at high strain rates along with the minimal structural damage under impact loading of the composites clearly show the potential of these novel structured materials for myriad shock absorption or damping applications.

In principle, the discussed approach can be generalized for any polymer matrix, including dispersion hardened polymer composites, and can be enacted at smaller length scales by selecting stiff balls of smaller diameters and by employing contactless methods to arrange balls in periodic arrays, such as by application of magnetic field if the stiff balls are magnetic<sup>29</sup>, etc. The energy absorption is to weight ratio of composites with the periodic array inclusions can be further enhanced by using bio-inspired design of double layered balls<sup>30</sup>, where inner metallic foam like core is uniformly coated with an optimized thickness of solid steel or other hard material. However, it should be noted that the mechanical behavior of the proposed composite architecture is expected to be different in the tension and the compression. This is evident as spheres come in contact and then slide over each other under compression loading whereas they will move away from each other in the tension precluding any strengthening due to the contact between spheres and an increase in the deformed volume of PDMS due to the sliding between two spheres. This behavior of the composite architecture is similar to the granular media<sup>31</sup>.

The mechanical behavior of PDMS and the steel ball filled PDMS composites were studied under quasi-static and dynamic loading conditions. The PDMS-steel ball composites showed superlative

**Table 2 | A comparison of effectiveness of different composite structures as compared to the base material in terms of energy absorption per unit volume**

System	Increase in Absorption Energy per Unit Volume, $\Gamma_{Composite}/\Gamma_{Base\ Material}$	Reference
Carbon Nanotube-PDMS layered composite	~1.5	27
Morten filled with ~5% of carbon nanotubes	~1.5	19
20% Glass fiber reinforced Nylon6/6 <sup>1</sup>	~0.4	28
20% Carbon fiber reinforced Nylon 6/6	~0.7	28
Quasi-isotropic carbon with PBO hybrid fiber	~2	18
PDMS-steel ball composite	~4.5	This work

<sup>1</sup>The nylon based composite data were derived using the damping coefficient at the temperature where they were maximum.

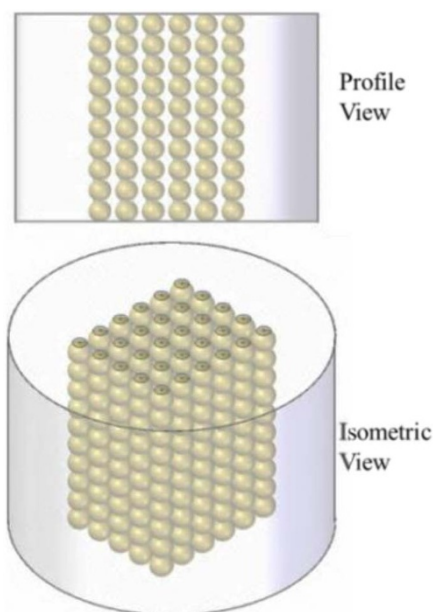


**Figure 6** | A schematic of the PDMS-steel ball composite.

mechanical behavior as compared to the monolithic PDMS samples—under quasi-static loading conditions, it showed both high stress for an imposed strain and the high energy absorption during the stress-strain hysteresis, and under dynamic loading condition, it not only retained the structural integrity but also showed orders of magnitude higher energy absorption capability. The deformation mechanism in these PDMS-steel ball composites consisted of: (i) sliding of the steel balls over each other, (ii) deformation of an additional volume of the PDMS during this sliding process providing the composite with an extra strength, and (iii) reversion back of the steel balls to their original position upon the removal of the load. The replacement of a continuous steel rod with multiple disjoint balls forming a periodic chain like structure is the key to the extraordinary shock absorption and damping behaviors of these PDMS-steel ball composites at both the low and the high strain rates.

## Methods

**Sample preparation.** PDMS monomer and the appropriate cross linker were mixed in a 10 : 1 ratio and then poured into an aluminum mold of 13.5 mm inner diameter and 11.7 mm height. Consequently, the fluid mixture was cured at 80°C for 60 minutes to produce the monolithic PDMS samples of the same dimensions as of the interior of the mold. For preparing PDMS samples with a periodic arrangement of the steel balls, the above mold was modified by affixing a 5 × 6 array of steel rods of 0.78 mm diameter and 20 mm length to its base. The center to center spacing between the steel rods was 1.5 mm. Following the curing of the PDMS in this modified mold, the steel rods were pulled out creating through holes of 0.78 mm diameter in the otherwise solid PDMS sample. Ten chrome-plated stainless steel balls of 1.17 mm diameter were mechanically inserted in the already existing holes in the cured PDMS resulting in a periodic stacking of balls in each hole. A schematic of the resulting PDMS-steel balls composite is shown in Fig. 6. Since the implantation of the steel balls inside the cured PDMS was purely mechanical, no chemical interaction via interfacial bonding occurred. Therefore, the chemical composition and behavior of the PDMS matrix of the PDMS-steel ball composite is expected to be same as that of the monolithic PDMS. The volume fraction of the steel in the prepared PDMS-steel ball composite was ~60%. The PDMS-steel ball composite samples had the same height and diameter as the monolithic PDMS samples.

**Quasi-static and high strain rate compression testing.** At first, both monolithic PDMS and the PDMS-steel ball composites were compressed to different engineering strains, ranging from 5 to 50%, at a nominal strain rate of 0.05 s<sup>-1</sup>. After compression to the set strains, the samples were unloaded at the same strain rate of 0.05 s<sup>-1</sup>. A few of the monolithic PDMS samples were also tested through another loading and unloading cycle to determine the effect of the cumulative damage accumulation on the stress-strain behavior of the polymer matrix. To minimize the effect of bulging while compressing these samples, an iron encapsulation with an inner diameter of 13.5 mm was placed around each sample. Even though this type of adaptation

produced hydrostatic stresses and hence tri-axial state of stress in the sample, it allowed continuation of these tests up to very large compressive strains. If the iron encapsulation was not placed, the transparent PDMS matrix allowed direct visualization of the movement of the steel balls during a mechanical test. Hence *in-situ* video imaging during a few of the tests was conducted with a standard optical camera operating at a rate of 20 frames per second.

A comparison of the behavior of these samples, *i.e.* monolithic PDMS and PDMS-steel ball composites, under dynamic or shock loading conditions was conducted using the split Hopkinson bar technique. After a sample was placed in a steel encapsulation attached to the split Hopkinson bar test set-up, an incident bar hit the sample and the signals pertaining to the strain rate and stress data were recorded. Reloading of the sample was precluded by attaching momentum traps to both the incident and the transmission bars. The tested samples were visually inspected for the signs of macroscopic damages. Strain rates of >2400 s<sup>-1</sup> were recorded during split Hopkinson bar test.

- Balazs, A. C., Emrick, T. & Russell, T. P. Nanoparticle-polymer Composites: Where Two Small Worlds Meet. *Science* **314**, 1107–1110 (2006).
- Thostenson, E. T., Ren, Z. & Chou, T. W. Advances in the science and technology of carbon nanotubes and their composites: a review. *Comp. Sci. Technol.* **61**, 1899–912 (2001).
- Qian, D., Dickey, E. C., Andrews, R. & Rantell, T. Load transfer and deformation mechanisms in carbon nanotube-polystyrene composites. *Appl. Phys. Lett.* **76**, 2868–2870 (2000).
- Dutta, *et al.* Liquid Phase Sintered Solders with Indium as Minority Phase for Next Generation Thermal Interface Material Applications. *J. Elect. Mater.* **38**, 2735–2745 (2009).
- Kumar, P. & Awasthi, S. Mechanical and Thermal Modeling of In-Cu Composites for Thermal Interface Materials Applications. *J. Comp. Mater.* DOI: 10.1177/0021998313486502.
- Heinrich, G., Kluppel, M. & Vilgis, T. A. Reinforcement of elastomers. *Current Opinion Solid State Mater. Sci.* **6**, 195–203 (2002).
- Hogg, P. J. Composites in Armor. *Science* **314**, 1100–1101 (2006).
- Sarva, S. S., Deschanel, S., Boyce, M. C. & Chen, W. Stress-Strain Behavior of a Polyurea and a Polyurethane from Low to High Strain Rates. *Polymer as a Communication* **48**, 2208–2213 (2007).
- Qiao, P., Yang, M. & Bobaru, F. Impact Mechanics and High-Energy Absorbing Materials: Review. *J. Aerospace Eng.* **21**, 235–248 (2008).
- Ward, I. M. & Sweeney, J. *An introduction to the mechanical properties of solid polymers.* (John Wiley and Sons Ltd., 2004).
- Medalia, A. I. Effect of Carbon Black on Dynamic Properties of Rubber Vulcanizates. *Rubber Chem. Technol.* **51**, 437–523 (1978).
- Heinrich, G. & Vilgis, T. A. Contribution of entanglements to the mechanical properties of carbon black-filled polymer networks. *Macromolecules* **26**, 1109–1119 (1993).
- Choi, S. S. Filler-polymer interactions in both silica and carbon black-filled styrene-butadiene rubber compounds. *J. Polym. Sci. B* **39**, 439–445 (2001).
- Fiedler, B., Gójny, F. H., Wichmann, M. H. G., Nolte, M. C. M. & Schulte, K. Fundamental aspects of nano-reinforced composites. *Comp. Sci. Technol.* **66**, 3115–3125 (2006).
- Yu, C., Gao, H., Yu, H., Jiang, H. & Cheng, G. J. Laser dynamic forming of functional materials laminated composites on patterned three-dimensional surfaces with applications on flexible microelectromechanical systems. *Appl. Phys. Lett.* **95**, 091108–091110 (2009).
- Landolt, J. H., Magalhaes, P. H., Nóvoa, P. R., Viana, J. & Marques, A. T. Low velocity impact of thermosetting composite systems modified with rubber and cork powders. *Sci. Eng. Comp. Mater.* **12**, 103–108 (2011).
- van der Jagt, O. C. & Beukers, A. The potential of a new rigid-rod polymer fibre (‘M5’) in advanced composite structures. *Polymer* **40**, 1035–1148 (1999).
- Larsson, F. & Svensson, L. Carbon, polyethylene and PBO hybrid fibre composites for structural lightweight armour. *Comp. A* **33**, 221–231 (2002).
- Koerner, H., Price, G., Pearce, N. A., Alexander, M. & Vaia, R. A. Remotely actuated polymer nanocomposites – stress-recovery of carbon-nanotube-filled thermoplastic elastomer. *Nature Mater.* **3**, 115–120 (2004).
- Paul, J., Sindhu, S., Nurmanwati, M. H. & Valiyaveetil, S. Mechanics of prestressed polydimethylsiloxane-carbon nanotube composite. *Appl. Phys. Lett.* **89**, 184101 (2006).
- Toki, S., Fujimaki, T. & Okuyama, M. Strain-induced crystallization of natural rubber as detected real-time by wide-angle X-ray diffraction technique. *Polymer* **41**, 5423–5429 (2000).
- Roynance, D. In *Engineering viscoelasticity* (2001) – date of access: 28<sup>th</sup> December, 2012. [web.mit.edu/course/3/3.11/www/modules/visco.pdf](http://web.mit.edu/course/3/3.11/www/modules/visco.pdf).
- Huang, R. C. & Anand L. In *Innovation in Manufacturing Systems and Technology* (IMST) (2005) – date of access: 28<sup>th</sup> December, 2012. <http://hdl.handle.net/1721.1/7456>.
- Boyce, M. C., Kear, K., Socrate, S. & Shaw, K. Deformation of thermoplastic vulcanizates. *J. Mech. Phys. Solids* **49**, 1073–1098 (2001).
- Quaglino, V. & Dubini, P. Friction of polymers sliding on smooth surface. *Adv. Tribology* **2011**, 178943 1–8 (2011).
- Li, J., Zhou, F. & Wang, X. Modify the friction between steel ball and PDMS disk under water lubrication by surface texturing. *Meccanica* **46**, 499–507 (2011).



27. Misra, A., Raney, J. R., De Nardo, L., Craig, A. E. & Daraio, C. Synthesis and characterization of carbon nanotube-polymer multilayer structures. *ACS Nano* **5**, 7713–7721 (2011).
28. Senthilvelan, S. & Gnanamoorthy, R. Damping Characteristics of Unreinforced, Glass and Carbon Fiber Reinforced Nylon 6/6 Spur Gears. *Polym. Test.* **25**, 56–62 (2006).
29. Jin, S., Tiefel, T. H. & Wolfe, R. Directionally-conductive, optically-transparent composites by magnetic alignment. *IEEE Trans. Magnetics* **28**, 2211–2213 (1992).
30. McKittrick, *et al.* Energy absorbent natural materials and bioinspired design strategies: A review. *Mater. Sci. Eng. C* **30**, 331–342 (2010).
31. Majumdar, T. S. & Behringer, R. P. Contact force measurements and stress-induced anisotropy in granular materials. *Nature* **435**, 1079–1082 (2005).

## Acknowledgements

Authors would like to thank Dr. Maen Alkhader of GLCIT, California Institute of Technology, Pasadena, CA (USA) for his help in conducting the high strain rate experiments. Financial support from IISc-JATP is acknowledged.

## Author contributions

A.M. designed and carried out the experiments. P.K. and A.M. analyzed the data and wrote the manuscript.

## Additional information

**Supplementary information** accompanies this paper at <http://www.nature.com/scientificreports>

**Competing financial interests:** The authors declare no competing financial interests.

**How to cite this article:** Misra, A. & Kumar, P. Periodic Architecture for High Performance Shock Absorbing Composites. *Sci. Rep.* **3**, 2056; DOI:10.1038/srep02056 (2013).



This work is licensed under a Creative Commons Attribution-NonCommercial-NoDerivs 3.0 Unported license. To view a copy of this license, visit <http://creativecommons.org/licenses/by-nc-nd/3.0>



DOI: 10.1038/srep03638

SUBJECT AREAS:

MECHANICAL  
ENGINEERING

POLYMERS

COMPOSITES

MECHANICAL PROPERTIES

SCIENTIFIC REPORTS:

3 : 2056

DOI: 10.1038/srep02056  
(2013)

Published:  
24 June 2013

Updated:  
8 January 2014

## **CORRIGENDUM:** Periodic Architecture for High Performance Shock Absorbing Composites

Abha Misra & Praveen Kumar

The Acknowledgements section in this Article is incomplete; it should also contain the following statement:

“We would also like to thank Dr. Chiara Daraio of ETZ Zurich and Dr. Jordan R. Raney of Baylor University, Waco for discussion and development of the idea and US Army Research Office (under ICB contract) for partial financial support.”